Journal of the European Ceramic Society **17** (1997) 1223–1230

PII: S0955-2219(96)00230-0
0955-2219/97/$17.00

Dopant Distribution and Grain Growth Control in $BaTiO_3$ Ceramics Doped with ZnO–SiO_2–P_2O_5

A. C. Caballero,[a] J. F. Fernández,[a] C. Moure,[a] P. Durán[a] and J. L. G. Fierro[b]

[a]Electroceramics Department, Instituto de Cerámica y Vidrio (CSIC), Carretera de Valencia Km. 24,300, 28500 Arganda del Rey, Madrid, Spain
[b]Instituto de Catálisis y Petroleoquímica, CSIC, 28049 Cantoblanco, Madrid, Spain

(Received 16 August 1996; revised version received 28 October 1996; accepted 11 November 1996)

Abstract

In the present work, high-density $BaTiO_3$ ceramics with homogeneous fine-grained microstructure have been obtained by incorporating small amounts of SiO_2, P_2O_5 and ZnO and sintering at temperatures between 1175 and 1225°C. Dilatometry and porosimetry tests showed that sintering starts at higher temperature (around 200°C higher) for the doped material. As a consequence, for the doped material porosity coalescence and removal is promoted while grain growth is inhibited during the first sintering step. SEM and TEM analysis did not reveal any secondary phases in the microstructure of the samples sintered below 1250°C. Grain growth control and microstructural homogeneity seem related to the dopant distribution. XPS analysis showed that the dopants are distributed on the surface of the $BaTiO_3$ particles before the temperature at which sintering starts is reached. The behaviour of the Curie temperature indicates that dopants are incorporated as a solid solution after sintering below 1250°C. This incorporation may lead to compositional changes at the grain boundaries which would be the origin of the lower AC grain boundary conductivity measured by complex impedance analysis and the observed low dielectric losses (well below 1%) of the doped samples. The dielectric characteristics of the doped materials, and the flat dependence of the permittivity with the temperature, make these materials very promising ones for X7R applications. © 1997 Elsevier Science Limited.

1 Introduction

Barium titanate ($BaTiO_3$)-based ceramics are largely used in the electronics industry. At present, their most important application is as dielectric layers in multilayer ceramic capacitors (MLCC).[1] Among these, capacitors with X7R specifications are greatly appreciated because of their high volumetric capacitive efficiency and the temperature-compensated capacitance response. In order to fit X7R characteristics, $BaTiO_3$ has to be modified by incorporating dopants in the dielectric material. Additives are also incorporated to decrease the sintering temperature of the ceramic, which leads to lower production costs of the MLCC devices. Therefore, composition and processing must be carefully controlled to provide the highest permittivity value possible, homogeneous fine-grained microstruc-ture and to allow the reduction of the sintering temperature.[1–3]

On the other hand, simultaneous additions of different oxides may give rise to the presence of compositional heterogeneities in the microstructure of the sintered ceramic. As a consequence of inhomogeneous processing and/or interaction between different oxides, a second phase may be formed even for additions below the solid solution limit. This effect is specially relevant for the grain boundary dopants, which have low solubility in $BaTiO_3$ and are typically located at the grain boundaries after sintering. These dopants should be homogeneously distributed along grain boundaries: however it is common to observe dopant heterogeneities which can limit their effectiveness.[2,4]

Recently, ZnO additions to ceramic $BaTiO_3$ have been reported to be very effective in order to control grain growth and reduce dielectric losses.[5] However, the minimum ZnO amount leading to homogeneous fine-grained microstructure was very sensitive to changes in the dopant distribution. Therefore, ZnO doping effects have to be examined in the presence of other dopant oxides in order to evaluate the effectiveness of ZnO as a grain growth inhibitor in $BaTiO_3$-based dielectric formulations. For this purpose, in the present work, ZnO, SiO_2 and P_2O_5 have been incorporated simultaneously to $BaTiO_3$. SiO_2 is a classic glass-forming additive which is often incorporated to form low-melting phases which promote enhanced sintering of the ceramic.[2,6] On the other

hand, small amounts of P_2O_5 have been recently reported to have a strong effect on the microstructure development of $BaTiO_3$.[7,8] Dielectric tapes are usually obtained by tape casting, when ester phosphate is used as dispersant for the slip preparation, a solid residue of P_2O_5 is incorporated in the ceramic. This doping drives the material to lower sintering temperatures and homogeneous fine-grained microstructures under certain circumstances.[7]

2 Experimental Procedures

A commercial grade $BaTiO_3$ (Elmic BT100, Rhône Poulenc SA) raw material with Ba/Ti = 1·000 was used for the present study. Dopant precursors were solid ZnO (Merck ref. 8849), ester phosphate (Merck ref. 820251) and colloidal silica (Cabot Corp. ref. Cab-O-Sil EH-5). The main characteristics of these products are reported elsewhere.[5–8] According to the above quoted works, composition was chosen to be 0·5 wt% of ZnO, 0·2 wt% of SiO_2 and 0·13 wt% of P_2O_5, referred to the $BaTiO_3$ content.

Doped powders were prepared by incorporating the appropriate amounts of zinc oxide and colloidal silica into a dispersion of $BaTiO_3$ in an isopropyl alcohol solution of ester phosphate. Dispersion was attained by vigorous stirring by means of a high speed turbine (6000 rpm). This step can modify the characteristics of the ceramic powder, by contributing to break powder agglomerates. Therefore undoped barium titanate was also dispersed in the same way, although no dopant compound was added. This allows direct comparison of the data obtained for undoped and doped materials in order to determine doping-related effects. Isopressed bars were preformed with 200 MPa pressure. Sintering was carried out in air, with heating and cooling rates of 3°C per min and 2 h soaking time.

Photoelectron spectra were acquired with a Fison ESCALAB 200R spectrometer equipped with a hemispherical electron analyser and Mg $K\alpha$ 120 W X-ray source. The powder samples were pressed into small aluminium cylinders and then mounted on a sample rod placed in a pretreatment chamber and outgassed at room temperature for 1 h. The pressure in the ion-pumped analysis chamber was below 3×10^{-9} Torr (1 Torr = 133·33 Pa) during data acquisition. The spectra were collected for 20 to 90 min, depending on the peak intensities, at a pass energy of 10 eV (1 eV = $1{\cdot}602 \times 10^{-19}$ J) which is typical of high resolution conditions. The intensities were estimated by calculating the integral of each peak after smoothing and subtraction of the 'S-shaped' background and fitting the experimental curve to a combination of Lorentzian and Gaussian lines of variable proportion. All binding energies (BE) were referenced to the adventitious C 1s line at 284·9 eV. This reference gave BE values within an accuracy of ± 0·1 eV.

Sintering behaviour was followed by means of shrinkage measurements (Adamel Lhomargy DI 24) and porosimetry (mercury porosimeter Autopore II 9220) tests. Shrinkage measurements were performed on compacted bars heated at the same rate as that for isothermal sintering probes. Porosimetry tests were also performed on compacted samples. In order to follow the porosity evolution at different temperatures, thermal treated compacts were held 1 min at the treatment temperature and cooled for measurement. Mercury pressure ranging from 4×10^{-3} up to 400 MPa allowed detection of porosity between tens of microns and nanometers.

Density of sintered samples was determined by the Archimedes' method. Microstructure of sintered samples was observed by SEM and TEM. Discs were sliced from the sintered bars for electrical characterization. Ag 30-Pd 70 paste was used for printing electrodes. Dielectric parameters as a function of frequency were determined by means of a vectorial impedance analyser model HP 4192-A.

3 Results and Discussion

3.1 Sintering behaviour and microstructure

Measured apparent density values as a function of sintering temperature are shown in Fig. 1. Doped materials (BTPSZ) reach high density values (around

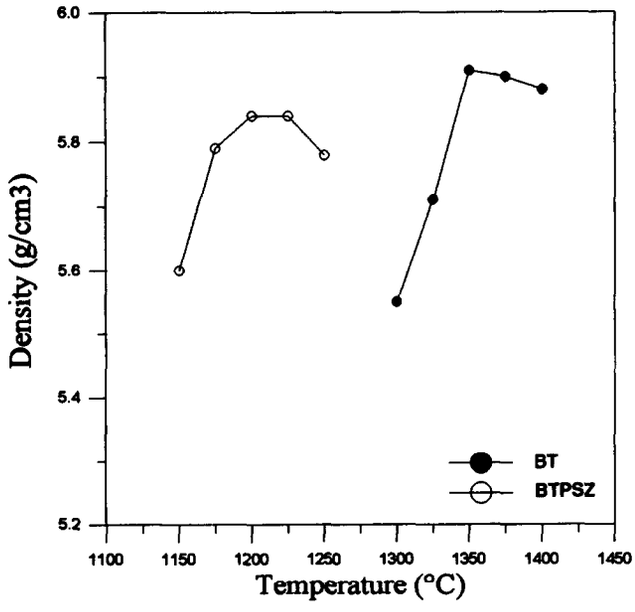

Fig. 1. Apparent density versus sintering temperature for doped (BTPSZ) and undoped (BT) materials.

97% D_t) starting from 1175°C and maximum density is obtained at 1200°C, 150°C lower than that for undoped $BaTiO_3$ (BT). Shrinkage rate curves (Fig. 2) also showed important differences. Sintering starts at higher temperatures for doped material, however, once it has started, sintering occurs much faster. Maximum shrinkage rate takes place 100°C lower for the doped material. Another important difference is that for undoped $BaTiO_3$ there is a noticeable slope change in the curve which is before the temperature of maximum shrinkage rate. On the other hand, in the case of the doped material, this change is detected at higher temperature than that of the maximum shrinkage. The behaviour of the undoped $BaTiO_3$ indicates that the reactivity of the powder leads to early densification (starting at 800°C) which prevents the efficient removal of porosity.[9] However for the doped material, porosity coalescence and removal is promoted in the first sintering step.

Porosimetry tests (Fig. 3) seem to confirm this point. For undoped $BaTiO_3$ the mean pore diameter increases from 0·16 μm for green compacts to 0·21 μm after thermal treatment at 1200°C. This indicates that porosity coalescence is still taking place at 1200°C. In the case of the doped material, the behaviour is quite different. The green compact shows a lower mean pore diameter of 0·10 μm and certain porosity in the range of 0·01 μm. Porosity coalescence takes place up to 1100°C increasing the mean pore diameter up to 0·16 μm, and small pores disappear. For compacts treated at 1200°C, mean pore diameter decreases

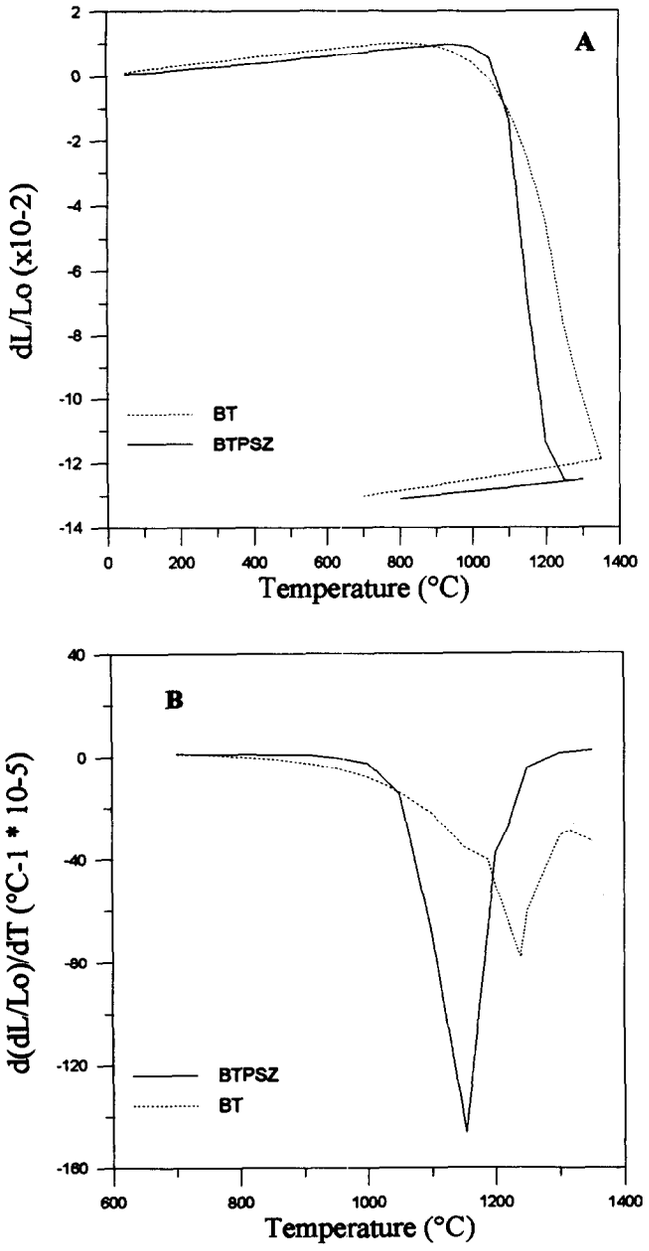

Fig. 2. Shrinkage rate versus temperature for doped and undoped materials.

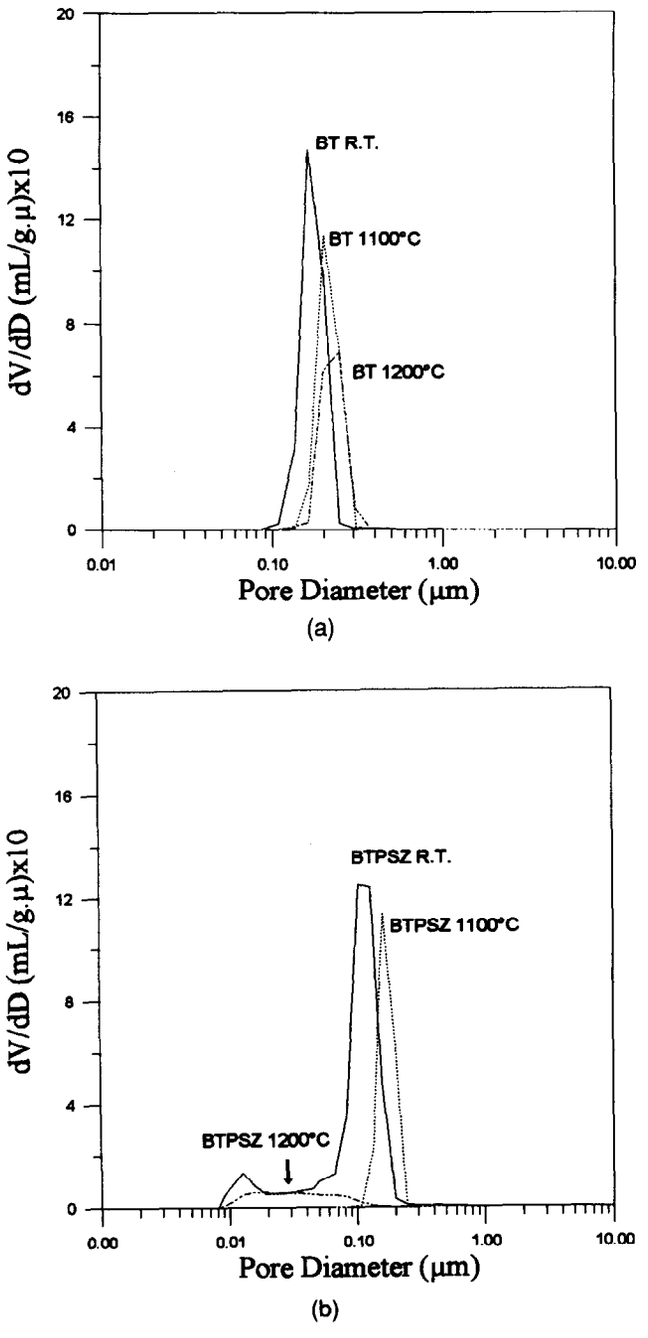

Fig. 3. Mean pore diameter for (a) undoped $BaTiO_3$ and (b) doped material treated at different temperatures.

up to 0·05 μm pointing to the end of the initial coalescence process. Moreover, the total porosity has largely decreased which also indicates that porosity removal is strongly improved.

SEM analysis of undoped $BaTiO_3$ samples (Fig. 4) shows that high density is reached only with important grain growth. Furthermore, anomalous grain growth was detected in all the undoped samples. The presence of intragranular porosity suggests that grain growth becomes relevant when porosity coalescence is still taking place, which corroborates the above discussion. On the contrary, doped materials sintered below 1250°C showed homogeneous fine-grained microstructure (Fig. 5(a)). High density values are reached with little grain growth as a consequence of improved porosity removal. A secondary phase is detected in the sample sintered at 1250°C (Fig. 5(b)), also grain growth is more marked in this sample. This effect seems to be reflected in the shrinkage rate curve as a sharp slope change, detected between 1200 and 1250°C (Fig. 2). Neither SEM nor TEM (Fig. 6) analysis revealed the presence of any secondary phase in the doped samples sintered below 1250°C. The domain pattern of TEM micrographs reveals that the periodic domains that transverse across the grains are not pinned at the grain boundaries, given a core-shell type structure.[7]

3.2 Grain growth and dopant distribution

According to the previous microstructural study, for the doped material it is not clear whether sintering (below 1250°C) occurs in the solid state or in the presence of a liquid phase. Although no second phase has been observed, the presence of a thin intergranular layer may remain undetected under the present characterization. Within this framework, grain growth control can be understood in two different ways. If sintering occurs in the solid state, then grain boundary motion may

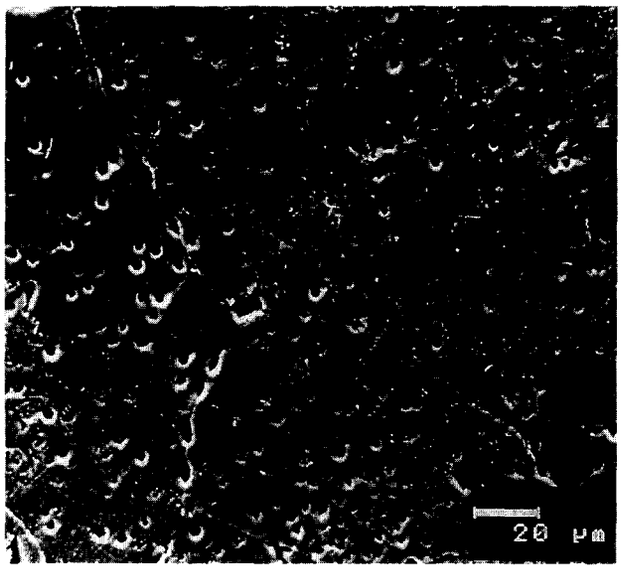

Fig. 4. SEM micrograph of polished and thermally etched surfaces of undoped $BaTiO_3$ sintered at 1350°C.

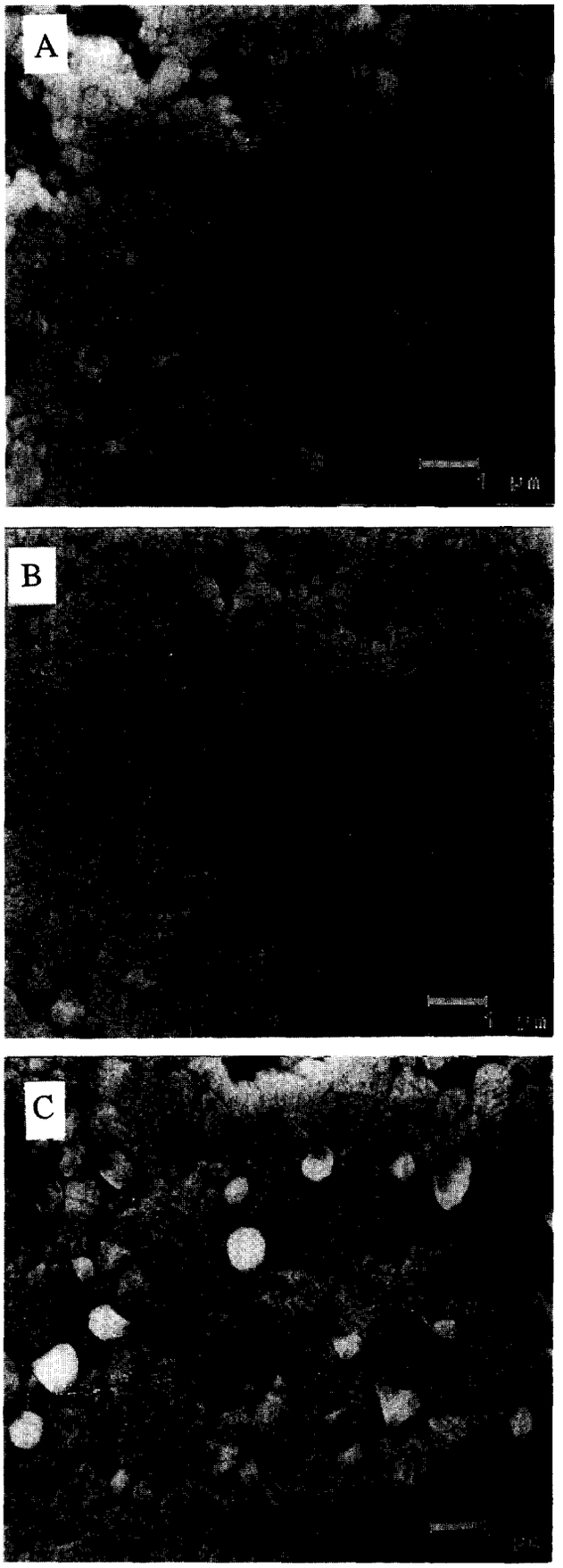

Fig. 5. SEM micrographs of polished and thermally etched surface of the doped samples sintered at (a) 1150°C, (b) 1200°C and (c) 1250°C.

be controlled by a solute drag mechanism. This is in agreement with previous results obtained regarding the low solid solubility of P^{5+}, Si^{4+} and Zn^{2+} into the $BaTiO_3$ lattice.[5,8,10] If this is so, for homogeneous microstructure to be reached, dopants should be well distributed along the surfaces of the $BaTiO_3$ particles before sintering starts, i.e. around 800°C according to the shrinkage rate curve for the undoped material. In this case, the microstructural features observed in the doped samples sintered below 1250°C indicate that after sintering the dopants should be incorporated into the grains to form a solid solution.

On the other hand, it has been recently proposed[7] that grain growth can also be controlled in the presence of a liquid phase. During sintering a transient liquid phase may form which improves particle packing and porosity removal. If the amount of liquid phase is small enough to avoid mass transport and is homogenously distributed covering the $BaTiO_3$ particles, then it is possible to reach high density and homogeneous fine-grained microstructure of the sintered ceramic. After sintering, this phase can be absorbed into the grains or grain boundaries to form a solid solution. Therefore, in this case the dopants would be also incorporated as a solid solution.

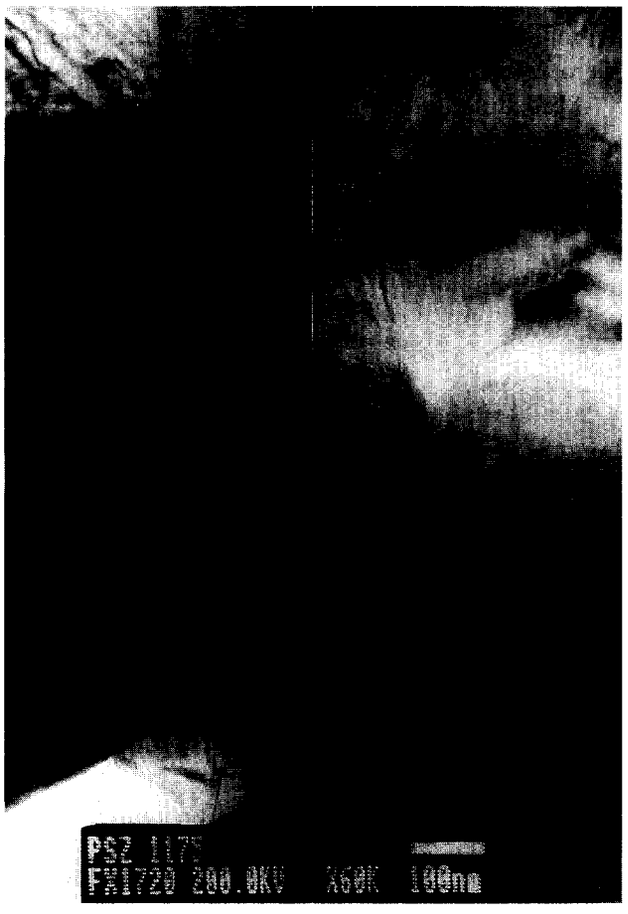

Fig. 6. TEM micrograph of the doped sample sintered at 1175°C.

In fact, taking into account the phase diagram of the system $BaTiO_3$–SiO_2[10] and the additional presence of P_2O_5 and ZnO in the material, local compositional changes may lead to liquid formation below 1250°C. Even if the overall amount of SiO_2 is below the solubility limit, its local concentration at certain areas of the sample may be high enough to give rise to liquid phase formation. Therefore, dopant distribution through the whole sample plays a critical role in order to reach homogeneous microstructure. This is obvious if sintering occurs in solid state but it is of similar importance if a liquid phase has been present. Since neither anomalous grain growth nor second phases have been detected in the doped samples sintered below 1250°C, the amount of liquid phase (if formed) must be very small and very well distributed in order to prevent mass transport during the first sintering step and to favour solid solution formation against phase separation during the last sintering step.

The Ti 2p, Ba 3d, Si 2p, Zn 2p, P 2p = 1s and C 1s core level spectra were recorded for the doped material previously treated at 700 and 1100°C. The binding energies of these levels are compiled in Table 1. The C 1s profile shows three components: a major one at 284·9 eV associated to hydrocarbon contamination, a second one of moderate intensity at about 286·1 eV coming also from residual contamination, and a minor one at 288·6–289·2 eV due to carbonate structures. The Ba 3d5/2 peak displays two components: a major one at 778·8 eV associated to BaO bonds in the oxide lattice, and a minor one at 780·2 eV characteristic of barium carbonate. The O 1s peak shows a major component at 529·4–529·7 eV due to lattice oxygen and two others at about 530·9 eV and somewhat about 534·4 eV due to hydroxyl groups and carbonate species, respectively. Finally, the binding energies of Ti 2p, Zn 2p, Si 2p and P 2p peaks were found typical of titanate, zinc, silicon and phosphorus oxides, respectively. Due to the strong insulator character of the sample, the quantification error is higher than usual in this technique and it is difficult to evaluate even though C 1s peak was used as reference. Consequently, the variations detected in the Ba/Ti ratio and the carbonated barium at the surface are too small to be discussed. However, the dopant

Table 1. XPS surface cations ratio for the doped $BaTiO_3$ powders

Sample	*Ba/Ti*	*Si/Ti*	*P/Ti*	*Zn/Ti*	$Ba_{carbonated}/Ba_{total}$
Formulated	1·000	0·008	0·003	0·025	—
400°C	1·007	0·041	0·170	0·030	0·33
700°C	0·984	0·053	0·137	0·063	0·42
1100°C	1·100	0·039	0·087	0·056	0·35

concentration at the surface of the $BaTiO_3$ particles is much larger than the average overall formulated concentration. According to previous works on SiO_2-[6] and P_2O_5-[8]doped $BaTiO_3$ this result is coherent with the doping procedure used for these materials. Dopant cations are clearly distributed along the surface of the particles. However, solid ZnO particles have been used as the source of Zn^{2+} cations, therefore these data indicate that ZnO has been redistributed along the surface of the $BaTiO_3$ particles. This occurs before 800°C, i.e. before sintering starts for the undoped material. The XPS data show that all the dopants are homogeneously distributed covering the $BaTiO_3$ particles just before sintering starts. In fact, this dopant distribution is the relevant one, since the distribution at room temperature (in the dried doped powder) can be modified by interactions between the different dopants. For the doped powder treated at 1100°C the dopants are still distributed along the surfaces, although the concentration is lower than that of the powder treated at 700°C. This may be related to the incorporation of the different dopants as a solid solution, or even with possible volatilization in the case of zinc and phosphorus.

3.3 Electrical properties

Dielectric constant and losses values, measured at room temperature and 1 kHz, are shown in Tables 2 and 3 for doped and undoped samples respectively. High permittivities are measured for both materials; however, the most important difference arises regarding the dielectric losses. The losses values are well below 1% for the doped samples sintered below 1250°C, around one order of magnitude lower than the values measured for undoped $BaTiO_3$. In the case of the doped sample sintered at 1250°C the dielectric losses increased above 1%, although they still remained much lower than the values observed for the undoped material. This may be related to the presence of the second phase detected during the study of its microstructure.

Figure 7 shows the grain boundary conductivity measured by the complex impedance technique. The strong overlapping between the bulk and grain boundary arcs did not allow to determine accurately the values associated to the grain interior. The behaviour of the grain boundary conductivity could be correlated with the dielectric losses values. Undoped samples showed the highest grain boundary conductivity and dielectric losses. The doped sample sintered at 1200°C, with no second phases detected in its microstructure, showed lower grain boundary conductivity and very low dielectric losses. However, the doped sample sintered at 1250°C showed lower grain boundary conductivity and dielectric losses than the undoped samples but higher than the doped ones sintered at lower temperatures. Therefore, it seems that the low level of dielectric losses detected in the doped samples originates from a less conductive grain boundary. This effect is larger in the samples for which no second phases were detected.

According to the curves of dielectric constant versus temperature (Fig. 8), the Curie temperature decreases 6°C for the doped materials sintered below 1250°C. For the doped material sintered at

Table 2. Dielectric constant and dielectric loss values measured at room temperature for doped materials sintered at different temperatures

Sintering temperature (°C)	ε′	*tan δ (%)*
1150	2729	0·68
1175	2630	0·53
1200	2452	0·62
1225	2354	0·52
1250	2481	1·06

Table 3. Dielectric constant and dielectric loss values measured at room temperature for undoped materials sintered at different temperatures

Sintering temperature (°C)	ε′	*tan δ (%)*
1300	3022	5·90
1325	2897	4·91
1350	3040	4·48
1375	2655	3·89
1400	2506	2·76

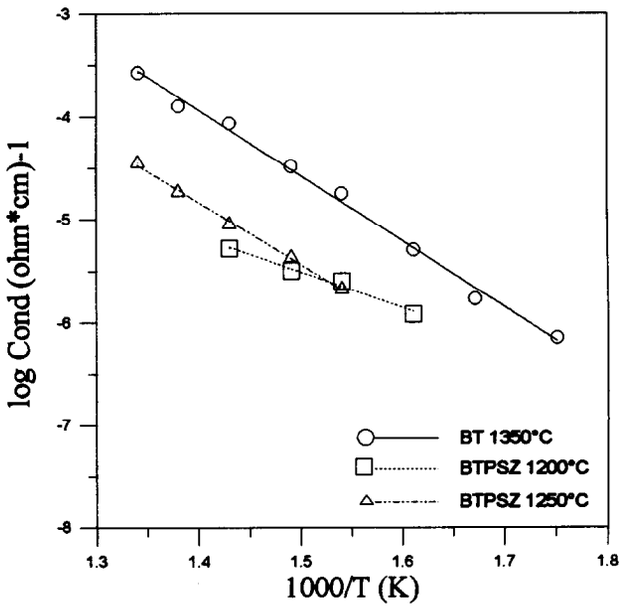

Fig. 7. Grain boundary conductivity versus temperature for undoped sample sintered at 1350°C and doped samples sintered at 1200°C and 1250°C.

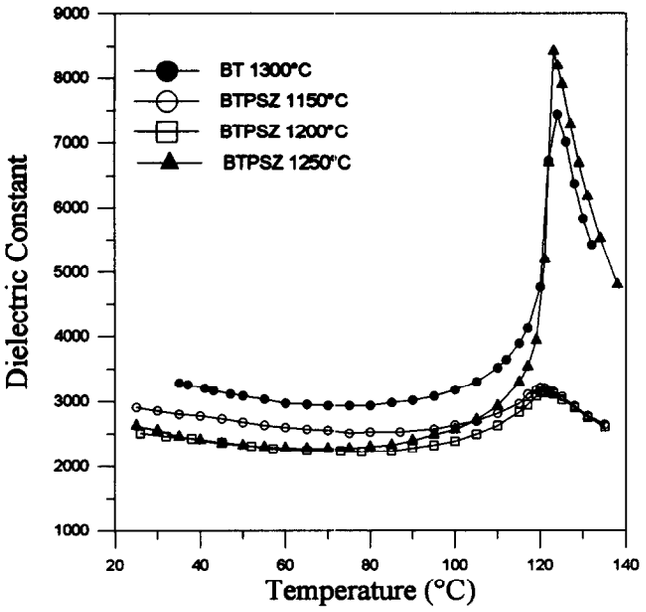

Fig. 8. Dielectric constant versus temperature for undoped sample sintered at 1300°C and doped samples sintered at different temperatures.

1250°C, the Curie temperature is only 2°C lower than for undoped $BaTiO_3$ and also the peak shape is much closer to the typical shape of undoped barium titanate. These results confirm that for the doped samples sintered below 1250°C, dopants are incorporated to form a solid solution. Initially the dopants are located on the particle surfaces in the doped powder, and they are incorporated into the $BaTiO_3$ lattice during sintering. Taking into account that low solubility into $BaTiO_3$ has been reported for these cations,[5,8,10] the dopant cations are expected to be located preferentially at the grain boundaries which could explain the domain pattern observed (Fig. 6). Both the higher disorder state due to dopant enrichment and the slow cooling rate that could partially relieve grain boundary stress allow the existence of a core-shell structure that reveals the higher stress provoked on the core regions due to the paraelectric-ferroelectric transition of regions with differences in composition. This change in the local grain boundary composition could be responsible for the lowering of its conductivity and therefore for lowering dielectric losses of the doped samples.

Conclusions

The simultaneous incorporation of SiO_2, P_2O_5 and ZnO to $BaTiO_3$ led to high density ceramics with homogeneous fine-grained microstructure for sintering temperatures ranging between 1175 and 1225°C. Doped samples sintered at 1250°C showed the presence of a second phase in the microstructure. Dilatometry and porosimetry tests showed that sintering starts at a temperature 200°C higher for the doped material. This improves the porosity coalescence and removal at the first sintering step and leads to a more homogeneous densification in which grain growth is initially inhibited.

There is no evidence about whether sintering takes place in the solid state or in the presence of a transient liquid phase. In any case, grain growth control only can be understood if dopants are homogeneously distributed covering the $BaTiO_3$ particles before sintering starts, otherwise exaggerated grain growth is expected to occur as in the undoped samples. XPS analysis of the doped powders treated at 700°C showed that, in fact, the dopant concentration at the surface of the particles is much higher than in the overall formulated composition. After sintering, dopants are incorporated into the $BaTiO_3$ as a solid solution in the samples sintered below 1250°C. According to previous results and the present data it is proposed that dopant cations are preferentially located at the grain boundaries changing the local composition. This could be the reason for the low grain boundary conductivity measured for these samples and the low level of dielectric losses (well below 1%) shown by these materials. The mentioned low dielectric losses together with a flat dependence of the dielectric constant on temperature make these materials very promising ones for X7R applications.

Acknowledgements

The authors are grateful to the Spanish Science Ministry for the financial support of this work (CICYT. MAT94-807).

References

1. Shepperd, L., Progress continues in capacitor technology. *Am. Ceram. Soc. Bull.*, 1993, **72**(3), 45–47.
2. Wilson, J. M., Minerals review—barium titanate. *Am. Ceram. Soc. Bull.*, 1995, **74**(6), 106–110.
3. Artl, G., The influence of microstructure on the properties of ferroelectric ceramics. *Ferroelectrics*, 1990, **104**, 217–227.
4. Schneider-Störmann, Vollmann, M. and Waser, R., Grain boundary decorated titanate ceramics: Preparation and processing. *Solid State Ionics*, 1995, **75**, 123–126.
5. Caballero, A. C., Fernández, J. F., Durán, P. and Moure, C., ZnO-doped $BaTiO_3$: Microstructure and electrical properties. *J. Eur. Ceram. Soc.*, in press.
6. Fernández, J. F., Durán, P. and Moure, C., Sintering and dielectric properties of SiO_2-doped $BaTiO_3$ ceramics. In *Euroceramics I*, vol. 2, ed. G. de With, R. A. Terpstra and R. Metselaar. Elsevier, Amsterdam, 1989, pp. 266–272.

7. Fernández, J. F., Caballero, A. C., Durán, P. and Moure, C., Improving sintering behavior of $BaTiO_3$ by small doping additions. *J. Mater. Sci.*, 1996, **31**, 975–998.
8. Caballero, A. C., Fernández, J. F., Moure, C. and Durán, P., Phosphorus-doped $BaTiO_3$: Microstructure development and dielectric properties. *J. Mater Sci.*, 1995, **30**, 3799–3804.
9. Hérard, C., Faivre, A. and Lemaitre, J., Surface decontamination treatments of undoped $BaTiO_3$—Part II; Influence on sintering. *J. Eur. Ceram. Soc.*, 1995, **15**, 145–153.
10. Rase, D. E. and Roy, R., Phase equilibria in the system $BaTiO_3$–SiO_2. *J. Am. Ceram. Soc.*, 1955, **38**(11), 389–395.